Critical shear stress for erosion of cohesive soils subjected to temperatures typical of wildfires

John A. Moody and J. Dungan Smith
U. S. Geological Survey, Boulder, Colorado, USA

B. W. Ragan
Department of Geosciences, Boise State University, Boise, Idaho, USA

Received 26 February 2004; revised 15 September 2004; accepted 5 November 2004; published 22 January 2005.

[1] Increased erosion is a well-known response after wildfire. To predict and to model erosion on a landscape scale requires knowledge of the critical shear stress for the initiation of motion of soil particles. As this soil property is temperature-dependent, a quantitative relation between critical shear stress and the temperatures to which the soils have been subjected during a wildfire is required. In this study the critical shear stress was measured in a recirculating flume using samples of forest soil exposed to different temperatures (40°–550°C) for 1 hour. Results were obtained for four replicates of soils derived from three different types of parent material (granitic bedrock, sandstone, and volcanic tuffs). In general, the relation between critical shear stress and temperature can be separated into three different temperature ranges (<175°C; 175°C–275°C; >275°C), which are similar to those for water repellency and temperature. The critical shear stress was most variable (1.0–2.0 N m^{-2}) for temperatures <175°C, was a maximum (>2.0 N m^{-2}) between 175° and 275°C, and was essentially constant (0.5–0.8 N m^{-2}) for temperatures >275°C. The changes in critical shear stress with temperature were found to be essentially independent of soil type and suggest that erosion processes in burned watersheds can be modeled more simply than erosion processes in unburned watersheds. Wildfire reduces the spatial variability of soil erodibility associated with unburned watersheds by eliminating the complex effects of vegetation in protecting soils and by reducing the range of cohesion associated with different types of unburned soils. Our results indicate that modeling the erosional response after a wildfire depends primarily on determining the spatial distribution of the maximum soil temperatures that were reached during the wildfire.

Citation: Moody, J. A., J. D. Smith, and B. W. Ragan (2005), Critical shear stress for erosion of cohesive soils subjected to temperatures typical of wildfires, *J. Geophys. Res.*, *110*, F01004, doi:10.1029/2004JF000141.

1. Introduction

[2] Increases in runoff and erosion are commonly observed after wildfires [*Doehring*, 1968; *Helvey*, 1980; *Moody and Martin*, 2001a]. However, to predict and model postfire erosion on a watershed scale (1–1000 ha) requires a quantitative understanding of the relation between the fundamental soil properties and the temperatures during a wildfire. Fire temperatures above the ground can range from 50°C to greater than 1500°C, but what in general is important to the biotic component of the soil is the heat released (typically 2×10^3 to 2×10^6 J kg^{-1} [*Neary et al.*, 1999]) and the subsequent heat flux into the soil (typically 2.4×10^3 W m^{-2} [*Massman et al.*, 2003]). Crown fires with large flame lengths may pass quickly and produce less heat flux into the soil than the combustion of the litter and duff layers, which often continue to burn long after the crown fire has passed [*Johnson and Miyanishi*, 2001]. Maximum temperature and heat flux also can change physical soil properties that affect erosion, such as organic matter content, pore volumes, aggregate stability, surface sealing, and permeability or saturated hydraulic conductivity [*Humphreys and Craig*, 1981; *Neary et al.*, 1999]. After a wildfire, a decrease in the hydraulic conductivity and hence in the infiltration rate has been postulated to be the result of fire-induced water repellency [*DeBano*, 2000]. However, it is important to remember that many soils are naturally water repellent [*DeBano*, 1969; *Doerr et al.*, 2000; *Dekker et al.*, 2001]. The degree of natural and fire-induced water repellency is related to the type of the soil particle size, organic matter, soil moisture, maximum temperatures, and duration of combustion [*DeBano and Krammes*, 1966; *DeBano*, 2000; *Doerr et al.*, 2000; *Robichaud and Hungerford*, 2000]. Laboratory measurements of *DeBano and Krammes* [1966] indicate that water repellency in granitic soils from southern California was a function of both maximum temperature and duration. However, the dependence on

0148-0227/05/2004JF000141$09.00

duration was within a narrow range between 5 and 20 min and for longer duration, water repellency was primarily a function of maximum temperature in the range from 150° to 480°C. Similarly, the presence or absence of cohesive forces in the soil produced by organic matter, clays, biological secretions [*Gerits et al.*, 1990], and organometallic compounds [*Giovannini et al.*, 1988] are dependent on temperature thresholds. Thus in general, maximum soil temperature is more important than total heat flux into the soil because both water repellency and cohesive forces are associated with temperature thresholds.

[3] Erosion of both cohesive and noncohesive soil consists of three separate processes. First is the separation, detachment, or initiation of motion of soil aggregates or particles from among neighboring aggregates or particles; second is the transport of these detached aggregates or particles; and third is an increase in the particle transport rate along a flow path (more generally a divergence of the particle transport rate) that results in removal of particles or aggregates from the hillslope. For example, a downhill flow of increasing depth on a uniform slope produces an increasing boundary shear stress and an increasing transport rate in the down-slope direction, hence a divergence of the sediment transport and erosion of the hillslope. These three processes can occur on hillslopes as a result of rain splash [e.g., *Poesen and Savat*, 1981], overland flow, a combination of these two processes [*Moss and Green*, 1983], or as a result of surface water from the adjacent hillslopes converging into drainages (unchannelized) and then into the channelized drainage network.

[4] Erodibility is commonly used in the literature to mean the inverse of the "resistance of the soil to both detachment and transport" [*Morgan*, 1986, p. 48] when subjected to an increasing force per unit surface area in the downhill direction. Erodibility has been expressed as a ratio of the mass of soil eroded per unit area per unit time per unit flow variable. Several different flow variables have been used such as kinetic energy per unit area [*Poesen and Savat*, 1981], rain intensity raised to a power [*Rose et al.*, 1983; *Elliot et al.*, 1989; *Flanagan and Nearing*, 1995], rainfall erosivity index [*Renard et al.*, 1997], unit stream power [*Rose et al.*, 1983; *Hairsine*, 1988; *Nearing et al.*, 1997], and force per unit surface area or boundary shear stress [*Elliot et al.*, 1989; *Flanagan and Nearing*, 1995]. Thus these formulations in the literature all fit the following general defining relation:

$$E = KX, \tag{1}$$

where E is the erosion of soil particles per unit area per unit time (kg m^{-2} s^{-1}), K is the erodibility, and X is a suitable flow variable. This definition makes the critical implicit assumptions that (1) the mass of eroded soil is linearly related to the chosen flow variable and (2) the erodibility is a constant property of a given soil. Three problems arise if erodibility is used to predict erosion on either unburned or burned hillslopes. First, the use of different flow variable for X makes it impossible to compare values of erodibility with differing dimensions of mass, length, and time. Second, the relation between eroded mass and the chosen flow variable is not linear over the entire range of any of these variables [*Meyer-Peter and Müller*, 1948; *Bathurst et al.*, 1987; *Hanson*, 1991; *Zhu et al.*, 2001], and as such erodibility is not a constant. Third, erodibility as defined by equation (1) includes both the initiation of motion process, which is soil property-dependent, and the transport process, which is not a fundamental property of the soil, but rather depends on the flow characteristics of the transporting fluid.

[5] By focusing on the three erosion-related processes separately, a theory for hillslope erosion after a wildfire can be developed. The logical choice is to first focus on the forces required to detach soil aggregates and particles, that is, on the initiation of motion for soil particles. Then, develop a theory for the transport and soil removal processes by spatially variable rainfall coupled with shallow flows on steep hillslopes. The transport theory, like those developed for clastic sediment transport [*Meyer-Peter and Müller*, 1948; *Yalin and Karahan*, 1979; *Wiberg and Smith*, 1987], will depend on the difference between the actual forces exerted by the flow on the soil aggregates (a property of the flow) and the forces required to initiate motion of the soil aggregates (a property of the soil).

[6] A few previous studies have focused on the initiation of motion of soil aggregates. For example, *Raudkivi and Tan* [1984] used an erosion model for cohesive soils [*Croad*, 1981] to determine the number of bonds per unit area and the activation energy to break interparticle chemical bonds of essentially pure clays. In contrast, *Nearing* [1991] developed a probabilistic model that incorporated the tensile strength of the soil, which is an aggregate measure of the resistant forces of both chemical and organic bonds. These resistant forces act per unit area on a hillslope or streambed, and thus they become stresses. Moreover, they are appropriately scaled by the boundary shear stress. Unit stream power has been used instead of boundary shear stress by *Yang* [1973], but it is proportional to the product of the boundary shear stress and the vertically averaged flow velocity. Particles or aggregates on the boundary at the threshold of motion, however, are not affected by the velocity field in the interior of the fluid. Rather, they are affected only by the near-boundary flow, which is scaled by the shear velocity (square root of the boundary shear stress divided by the fluid density). Consequently, the lift and drag forces on soil particles or aggregates, which both depend of the square of the velocity averaged over the site of the particle with the particle removed, are both scaled by the boundary shear stress.

[7] Boundary shear stress, τ_b, is the force per unit area exerted on the surface beneath the flow in the direction of the flow [*Middleton and Southard*, 1984]. It is used in cohesive sediment transport problems (such as those pertaining to marine clays with high water content) because it represents the direct force per unit area on the deforming pseudo-plastic [*Johnson*, 1970] mass. In contrast, it is used in clastic sediment transport problems because it is directly related to the drag and lift forces exerted by turbulent flows on objects protruding from the boundary such as sediment grains [*Middleton and Southard*, 1984; *Wiberg and Smith*, 1987]. Therefore when used for soils it scales both the force on the broad surface of a cohesive soil and the fluid forces (drag and lift) on particles composing that surface. At the threshold of particle motion, the critical boundary shear stress measures the force per unit area of surface required to break both the chemical and organic bonds among the soil

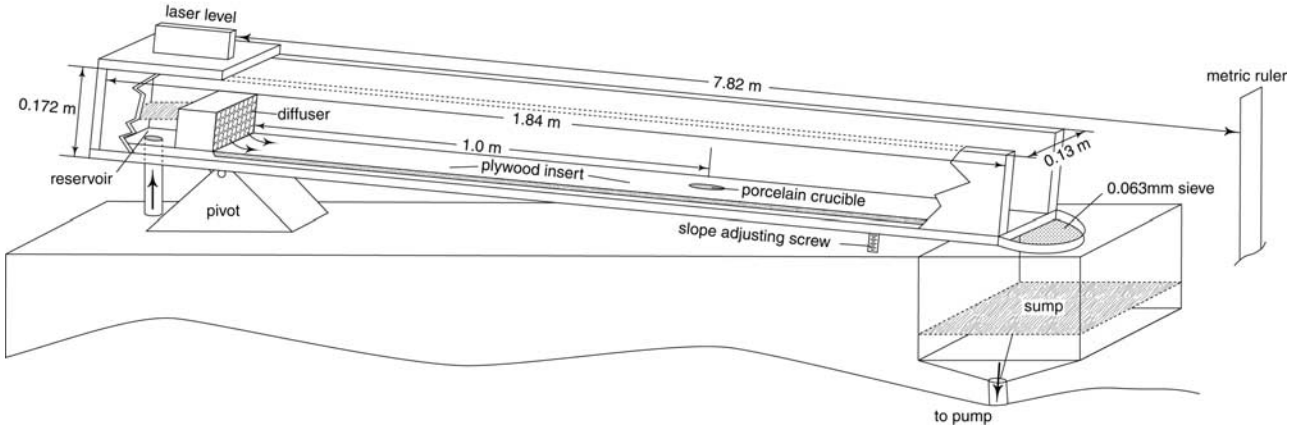

Figure 1. Experimental flume used to measure critical shear stress of forest soils.

particles composing the flow boundary. This critical shear stress for the initiation of soil motion may be the result of a high-velocity lateral flow associated with direct raindrop impact on the sediment surface [*Hartley and Julien*, 1992], raindrop impact through a thin water film covering the sediment surface, the force per unit area caused by turbulent overland flow, or a combination of these forces per unit bed area. By whatever means the force per unit area is applied to the boundary, the response of the boundary at the initiation of soil erosion can be measured by the value of the critical shear stress. As such, the critical shear stress for erosion is a property of the soil and not of the flow.

[8] Conceptually, the critical shear stress for a mixed-grain, cohesive soil differs from the critical shear stress for a noncohesive soil. It represents an aggregated property of the soil matrix rather than a property of a size specific, noncohesive particle setting in a pocket composed of similar particles and held there only by gravity (see *Wiberg and Smith* [1987] for a comprehensive discussion of the latter case). The hierarchical nature of the cohesive mechanisms (electrostatic-clay and sesquioxide-cement bonds at the 0.2 μm scale, encrustations of organic secretions and microbial debris at the 2 μm scale, and rhizomes and roots at the 200 μm scale [*Gerits et al.*, 1990]) results in soils with complex cohesive properties. Nevertheless, when the critical shear stress for erosion is measured, the number, types, and magnitudes of the forces resisting particle motion are not important, and the critical shear stress for soil particle motion becomes an aggregate measure of the forces that resist particle movement in the soil sample. The purpose of our study was to focus on the initiation of erosion process and to determine the change in the critical shear stress for several different mixed-grain, cohesive forest soils subjected to temperatures similar to those experienced by soils in wildfires.

2. Methods

2.1. Experimental Flume

[9] The critical shear stress for cohesive, forest soils subjected to different temperatures was measured in a 1.84 m long recirculating flume made from 12 mm clear plastic. The flume was 0.095 m wide and 0.158 m deep with a headbox and diffuser at one end and open at the other end such that water spilled into a sump and was circulated by a pump back to a reservoir (Figure 1). A plywood, bottom insert (0.095 m wide by 0.016 m thick by 1.5 m long) was place on the floor of the flume with an oval slot cut in the center of the plywood so that the top edge of a porcelain crucible (0.020 m wide, 0.105 m long, and 0.012 m deep) could be mounted flush with the top of the plywood insert. The test section was an area (0.017 m wide by 0.087 m long) within the crucible. This test section was located 1.0 m downstream from the end of the diffuser. Additional sidewalls (one plywood and one clear plastic) were clamped to the inside of the main sidewalls of the flume to hold the plywood bed in place. This reduced the width of the flume to 0.083 m. The flume rested on a pivot near the diffuser and the slope was adjusted by turning a vertical screw supporting the flume near the open end. Flow depths, h, ranged from 0.003 to 0.015 m, and the width-to-depth ratio ranged from 10 to 40. The bed roughness was greater than the sidewall roughness so that the sidewall effect upon the measured shear stress at the center of the flume was estimated to be less than 10%, using the method of *Shimizu* [1989].

2.2. Flume Calibration

[10] Calculating the boundary shear stress from measurements of water depth and slope was uncertain. One source of error was the nonuniform flow, which appeared to weakly accelerate or decelerate during some test cases; a second source was the form drag on the edges of the crucible, which was imbedded into the plywood bottom insert; and a third source was the error in measuring the shallow-flow depth, which was in many cases unacceptably large, possibly up to 20%. Thus the test section was calibrated to determine the boundary shear stress for combinations of water discharge and slope of the flume using well-sorted, noncohesive sediment mostly from a stream in a local burned watershed (Table 1). Critical shear stress for well-sorted, noncohesive sediment has long been established from flume measurements [*Shields*, 1936; *Yalin and Karahan*, 1979], but in all experiments, it has required a subjective criterion. The criterion for the initiation of motion used in this paper was the initiation of significant particle motion. This was defined to be the movement of particles from different locations at different times within the test

Table 1. Particle Size Classes and Theoretical Critical Shear Stress of Noncohesive Sediments for Flume Calibration[a]

Size class			Critical Shear Stress					
Phi range	Lower, mm	Upper, mm	Lower, N m^{-2}	Upper, N m^{-2}	Mean Shear Stress, N m^{-2}	Discharge, L s^{-1}	Angle of Repose, deg	Sediment Source
4.0–3.5	0.062	0.088	0.16	0.22	0.19	0.102	62	fluvial
3.5–3.0	0.088	0.125	0.22	0.26	0.24	0.102	62	fluvial
3.0–2.5	0.125	0.180	0.26	0.29	0.28	0.102	62	fluvial and beach
2.5–2.0	0.180	0.250	0.29	0.33	0.31	0.102	62	fluvial and beach
2.0–1.5	0.250	0.355	0.33	0.37	0.35	0.102	62	fluvial and beach
1.5–1.0	0.355	0.500	0.42	0.48	0.45	0.102	67	colluvial
1.0–0.5	0.500	0.710	0.48	0.58	0.53	0.102	67	colluvial
0.50–0.25	0.710	0.850	0.58	0.72	0.65	0.102	67	colluvial
0.25–0.00	0.850	1.000	0.72	0.79	0.76	0.102	67	colluvial
0.00 to −0.25	1.000	1.18	0.79	0.99	0.89	0.102	67	colluvial
−0.25 to −0.50	1.18	1.40	0.99	1.14	1.07	0.102, 0.505	67	colluvial
−0.50 to −0.75	1.40	1.70	1.14	1.54	1.34	0.102, 0.505	67	colluvial
−0.75 to −1.00	1.70	2.00	1.54	1.75	1.65	0.505	67	colluvial
−1.00 to −1.25	2.00	2.36	1.75	2.26	2.01	0.505	67	colluvial
−1.25 to −1.50	2.36	2.80	2.26	2.61	2.44	0.505	67	colluvial

[a]Critical shear stress based on work of *Wiberg and Smith* [1987].

section such that there was a continuous flux of sediment downstream from the sample in the crucible. It is important to understand that significant motion is not the same as first motion used by some investigators. First motion is a time-dependent variable, and, as such, given enough time a particle may eventually move [*Miller et al.*, 1977; *Lavelle and Mofjeld*, 1987]. Significant motion is independent of time and thus less ambiguous. Owing to the shallow depths and high velocities used in the experiments, the criterion above excludes erosion by sweeps, which are small-scale, localized phenomena, and erosion of particles from pockets with lower than average angles of repose.

[11] The shallow flow in the flume imposed additional restrictions. The relative roughness, D/h, (where D is the particle diameter) was kept less than about 0.3 by using two separate discharges (0.102 L s^{-1} ±3.5% and 0.505 L s^{-1} ±9.2%). This restriction was necessary because for larger values of D/h, the forces on the particles in the flume were no longer scaled just by the boundary shear stress. Instead, they also depended on the velocity profile, which depended, in turn, on the nature of the roughness of the bed [*Wiberg and Smith*, 1987]. When the relative roughness (D/h) is less than about 0.3 this effect can be ignored [*Ashida and Bayazit*, 1973; *Govers*, 1987].

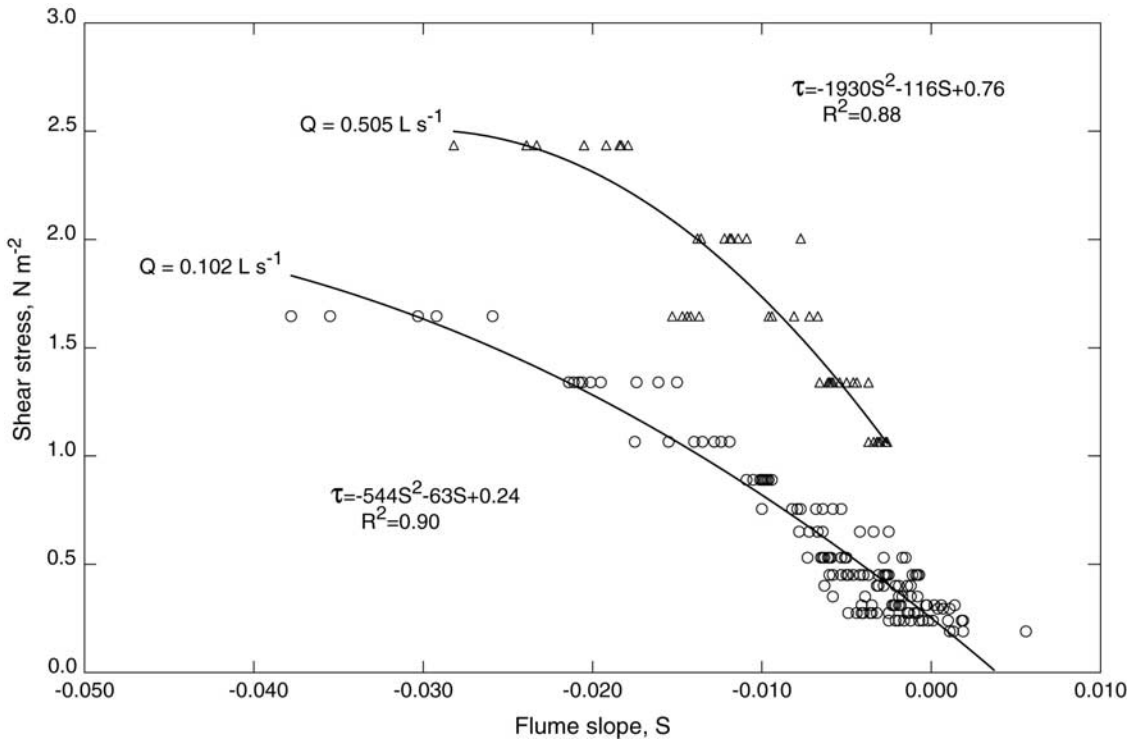

Figure 2. Two calibration curves for the flume with a discharge of 0.102 and 0.505 L s^{-1}. Multiple replicates of 15 different size classes of sand and gravel were used to construct these calibration curves. Polynomial regression equations were the best fit (largest R^2) to the data and are shown on the graph.

[12] As mentioned above, the measurement site in the flume was calibrated by observing the initiation of significant motion of well-sorted, noncohesive sediment particles, measuring the corresponding flume slope, and calculating the critical shear stress. Measurements of the slope of the flume were repeated at least five times for each size class of noncohesive particles. Critical shear stress was computed (see equation (9) below) using the theory of *Wiberg and Smith* [1987]. Shear stress was computed for the lower and upper particle diameter of each size class. The average of these two values was used to represent the critical shear stress of the entire size class because each size class had a relatively narrow range of particle diameters. Four plywood bottom inserts (with the slot for the crucible) were used alternately and calibration runs were made for each size class of noncohesive particles using each of these inserts. Fluvial and beach sand was used for size classes less than 0.355 mm rather than the sediment from the burned watershed because the latter, noncohesive sediment had significant amounts of plate-like mica particles that detach quickly and obscure the view of the sand grains. A total of 236 runs were made to calibrate the flume slope to the theoretical critical shear stress (Figure 2).

2.3. Critical Shear Stress Theory

[13] The critical shear stress for noncohesive sediment particles was calculated using the theory of *Wiberg and Smith* [1987]. Briefly, the forces in the direction of flow acting to move a noncohesive particle that is underwater are (1) the fluid drag, F_D, and (2) the down-slope component of the gravitational force on the particle minus the buoyancy, namely the effective weight of the particle in water, $F_g' \sin\theta$. Here, θ corresponds to the local inclination of the flume bed or the forest floor. The force acting to resist the particle motion is the bed-normal component of the effective weight, $F_g' \cos\theta$, holding the particle in a pocket in the surface composed of other particles. The component of the effective weight of the particle normal to the surface is decreased by the lift force, F_L, created by the square of the velocity difference between the bottom and the top of the particle (with the particle removed). The resulting effective weight, $F_g' \cos\theta - F_L$, is converted into a force parallel to the flume bed or the forest floor by multiplying by the tangent of the angle to which the surface would have to be tipped for the particle to roll out of its pocket. This is the same as the particle pocket angle, ϕ_0. Therefore the force balance on the particle in the direction of flow is

$$F_D + F_g' \sin\theta = \left(F_g' \cos\theta - F_L\right) \tan\phi_0, \tag{2}$$

which can be rearranged to yield equation (6) given by *Wiberg and Smith* [1987]:

$$F_D = F_g' \frac{\tan\phi_0 \cos\theta - \sin\theta}{1 + \tan\phi_0 (F_L/F_D)}. \tag{3}$$

The drag force on the particle is

$$F_D = 0.5\rho C_D \langle u^2 \rangle_A A_x, \tag{4}$$

where C_D is the particle drag coefficient for the particle, ρ is the density of water, $\langle u^2 \rangle_A$ is the square of the velocity of the fluid averaged over the cross-sectional area of the particle exposed to the flow with the particle removed, and A_x is the cross-sectional area of the particle perpendicular to the flow direction. The lift force on the particle is

$$F_L = 0.5\rho C_L \left(u_T^2 - u_B^2\right) A_z, \tag{5}$$

where C_L is the particle lift coefficient, u_T^2 and u_B^2 are the square of the fluid velocity that would be at the top and bottom of the particle were the particle removed, and A_z is the cross-sectional area of the particle of diameter D on the bed. The effective weight, F_g' is $(\rho_s - \rho) g V_s$, where ρ_s is the density of the particle, g is the acceleration due to gravity, and V_s is the volume of the particle. One common assumption is that the velocity near the soil surface varies in accordance with the law-of-the-wall (logarithmically with distance above the flow boundary) such that

$$u = \left(u_*/\kappa\right) \ln(z/z_0), \tag{6}$$

where u_* is the shear velocity ($u_* = (\tau_b/\rho)^{1/2}$), κ is von Karman's constant (0.408), z is the distance above the soil surface, and z_0 is an effective hydraulic roughness parameter. However, close to the boundary, viscosity effects (ν is the kinematic viscosity, $m^2\ s^{-1}$) become important and we used the *Reichardt* [1951] equation, which yields a linear velocity profile within the viscous sublayer ($z \ll \delta_\nu = 11.6\nu/u_*$) with the thickness of the sublayer given by δ_ν(m), and logarithmic profile above the viscous sublayer

$$u = u_* \left\{ \left[\frac{1}{\kappa} \ln\left(1 + \frac{\kappa u_* z}{\nu}\right) \right] - \left(\frac{1}{\kappa} \ln\left(\frac{u_* z_0}{\nu}\right) + \ln\kappa \right) \cdot \left(1 - e^{-u_* z/11.6\nu} - \frac{u_* z}{11.6\nu} e^{-\frac{0.33 u_* z}{\nu}}\right) \right\} = u_* f_R(\kappa, \nu, z_0, z). \tag{7}$$

The term inside the brackets is a form of the law-of-the-wall, the other term is a result of the viscous effects, and all the terms inside the curly brackets are abbreviated as f_R. The average of the square of the velocity over the cross-sectional area of the particle exposed to the flow is therefore

$$\langle u^2 \rangle_A \cong u_*^2 \int_{z_b}^{D+z_b} f_R^2(\kappa, \nu, z_0, z) dz = u_*^2 I_R, \tag{8}$$

where the integral, I_R, is approximated here by assuming a square instead of a circular cross section. Here z_b is the distance of the bottom of the particle above the level at which the flow velocity is zero ($z = z_0$). Usually z_b is negative and thus the integration begins at z_0.

[14] Substituting expressions for F_D, F_L, and F_g' into equation (3) and using the relation $\tau_b = \rho u_*^2$ gives the theoretical equation for the critical shear stress

$$(\tau_b)_c = \frac{(\rho_s - \rho) g \alpha_1 D \cos\theta (\tan\phi_0 - \tan\theta)}{I_R C_D \left[1 + \tan\phi_0 \left(\frac{C_L}{C_D} \frac{\left(f_T^2 - f_B^2\right)}{I_R}\right)\right]}, \tag{9}$$

where we have assumed that $A_x = A_z$ and set $2V_s/A_x = \alpha_1 D$ ($\alpha_1 = 4/3$ for spherical and = 1 for cubic particles).

Table 2. Soil Properties of Unburned, Burned, and Eroded Samples[a]

Site	USGS 7.5 min Quadrangle	Section Township Range	Bedrock Type	Bulk Density, g cm^{-3}	Percent Loss on Ignition at 550°C	n	Percent Silt and Clay <0.063 mm	Percent Sand 0.063–2.0 mm	Percent Gravel >2.0 mm	D_{50}, mm With <0.063 mm	D_{50}, mm Without <0.063 mm	Ratio D'_{50}/D_{50} Without <0.063 mm
					Unburned							
Hi Meadow	Windy Peak	7, T8S, R71W	granite	1.3 ± 0.0	7.3 ± 2.3	9	4 ± 1	71 ± 4	25 ± 4	0.9 ± 0.1	1.0 ± 0.1	0.9 ± 0.1
Rendija[b]	Guaje Mountain	3, T19N R6E	volcanic tuff volcanic tuff	1.2 ± 0.1	6.0 ± 3.6	6	10 ± 5	61 ± 20	29 ± 20	2.0 ± 2.8 0.5[c] ± 0.1	2.4 ± 2.9 0.9[c] ± 0.6	nm 0.7[c] ± 0.2
Pine Ridge	Golden	17, T3S, R70W	sandstone	1.1 ± 0.1	6.0 ± 3.6	3	7 ± 0.8	89 ± 3	4 ± 3	0.2 ± 0.0	0.2 ± 0.0	1.1 ± 0.1
RMHRC	Allenspark	24, T3N, R73W	granite	1.2 ± 0.1	7.0 ± 1.8	3	14 ± 1	85 ± 1	1 ± 1	0.2 ± 0.0	0.3 ± 0.0	1.0 ± 0.1
					Burned							
Hi Meadow	Windy Peak	7, T8S, R71W	granite	1.5 ± 0.1	nm	10	8 ± 3	39 ± 4	53 ± 7	2.3 ± 0.6	nm	nm
Rendija	Guaje Mountain	3, T19N, R6E	volcanic tuff	1.0 ± 0.1	nm	6	22 ± 3	59 ± 10	19 ± 11	0.5 ± 0.5	nm	nm
Hayman	Cheesman Lake	17, T10S, R71W	granite	1.2 ± 0.1	5.8 ± 4.3	4	6 ± 6	43 ± 5	51 ± 11	2.2 ± 0.9	2.5 ± 0.8	0.3 ± 0.1
Missionary	Rules Hill	27, T36N, R7W	sandstone	1.0 ± 0.1	7.4	1	27	50	23	0.1	0.1	3.8 ± 0.3

[a]Abbreviations are as follows: n, number of measurements; D'$_{50}$, eroded sediment from heated sample; values following the ± symbol are 95% confidence limits; nm, not measured.
[b]These soils have a bimodal distribution, which is indicated by the large confidence limits; the D_{50}s are about 0.6 mm and 9.1 mm.
[c]These calculations did not include the single sample with D_{50} = 9.1 mm.

[15] The pocket angle, ϕ_0, was determined as a function of particle size for classes (0.125 to 2.86 mm) sieved from noncohesive sediments that had eroded from hillslopes and channels after rainstorms following the Buffalo Creek Fire in Colorado in 1996 [*Moody and Martin*, 2001b]. These sediment particles were chosen as having a shape more typical of particles composing soils. The relation between the particle pocket angle (in degrees) and the ratio, D/k_s, of the moving particle diameter, D, on a bed composed of particles with median diameter, k_s, according to *Miller and Byrne* [1966] is

$$\phi_0 = \phi_1 (D/k_s)^{-\beta}, \tag{10}$$

where β is a sorting parameter. For sands eroded after a rainstorm over the watersheds burned by the Buffalo Creek Fire, $\phi_1 = 67°$ and $\beta = 0.31$. At the 25th and 75th percentiles, the values were $\phi_1 = 56°$ and $\phi_1 = 81°$, respectively. According to the measurements of *Miller and Byrne* [1966]$\phi_1 = 70°$ and $\beta = 0.3$ for angular sediment (typical of the hillslopes of concern). The median value was used to calculate the theoretical critical shear stress for the upper and lower limits of each size class using equation (9) (Table 1). The geometry of the pocket angle, ϕ_0 has been related to z_b by *Wiberg and Smith* [1987] with the equation

$$\phi_0 = \cos\left(\frac{(D/k_s) + z_*}{(D/k_s) + 1}\right), \tag{11}$$

where $z_* = z_b/k_s$. The flume was calibrated using well-sorted particle size classes (Table 1) consequently $D/k_s = 1$ and using $\phi_0 = 67$ gives $z_* = -0.22$, which is similar to the value (−0.16) for "crushed quartz" determined by *Wiberg and Smith* [1987], such that in both cases the bottom of the particle is below the level where the velocity is zero.

2.4. Soil Properties

[16] Forest soils were collected from four unburned and four burned sites in Colorado and New Mexico, and represent three different bedrock parent materials. Samples from unburned sites were collected from soils derived from granitic (Hi Meadow and Rocky Mountain Hydrologic Research Center or RMHRC sites (Table 2)) and sandstone bedrock (Pine Ridge site) in the Colorado Front Range, and from soils derived from welded and nonwelded volcanic tuffs in New Mexico's northern Jemez mountains (Rendija site). Samples from burned sites were collected from granitic soils (Hi Meadow and Hayman sites) in the Colorado Front Range, from sandstone soils (Missionary site) in San Juan mountains of southern Colorado, and from welded and nonwelded volcanic tuffs soils in the Jemez mountains (Rendija site). Cohesion in forest soils is predominately a function of organic content and particle size. Therefore the organic content was measured as loss on ignition at 510°–550°C for 1 hour [*DeBano and Conrad*, 1978; R. Stallard, written communication, 1998] and was found to be similar among all samples (Table 2). The particle size

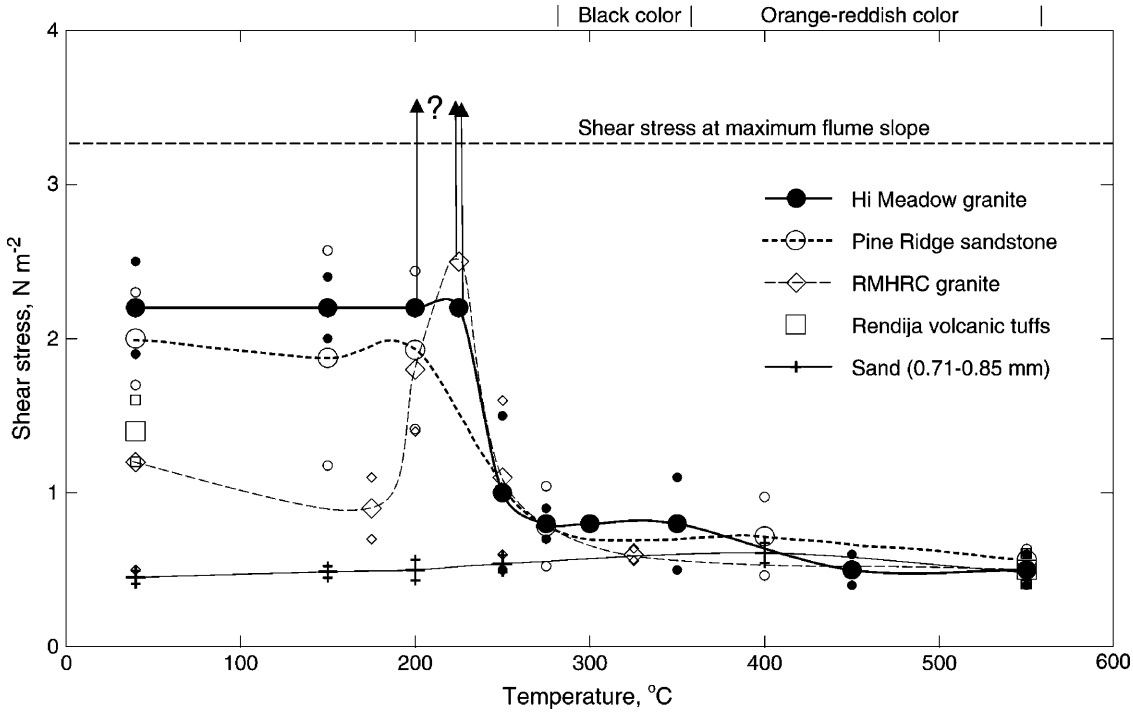

Figure 3. Critical shear stress for initiation of erosion of three types of forest soils (granite, sandstone, and volcanic tuffs). Smaller symbols indicate the 95% confidence limits for the mean of replicate samples shown by the larger symbol (some limits do not show because larger symbols are superimposed (see Table 3)). The question mark indicates that the critical shear stress measurements are a minimum and are certainly much greater than the upper limit of 3.2 N m^{-2} shown on the graph.

distribution of the remaining mineral soil was determined by sieve analysis (Table 2).

2.5. Soil Sample Preparation

[17] Multiple soil samples were collected in the field as intact box cores, placed in aluminum protective containers, and later subsampled for testing in the laboratory. One side of the thin, aluminum protective container was carefully removed from a field sample (0.2 m × 0.2 m × 0.05 m), subsamples were cut from the field sample, and mounted in a crucible for heating and testing in the flume. To help maintain the integrity of the subsample during the cutting and transfer process, the field sample was wetted for about 1 hour before starting the process. Four subsamples from the same field sample were put in four separate crucibles, placed in a preheated muffle furnace at the same temperature for 1 hour, and then tested in the flume to provide replicate measurements. If there was not enough soil in the field sample for four subsamples, then another field sample was used. The relatively narrow and shallow crucibles insured that the entire subsample was subjected to the specified temperature, which was verified using the soil temperature equation given by *Koorevaar et al.* [1983]. Temperature fluctuations of the muffle furnace were about 1%. To insure that the subsample was flush with the top of the crucible after being heated to temperatures greater than 300°C, the sample was cut and placed in the crucible such that 0.001–0.002 m of soil was above the top edge of the 0.012-m-deep crucible. This compensated for the settling during heating caused by a decrease in bulk density (≈−20% ≅ −0.002 m/0.012 m). For subsamples subjected to temperatures less than 300°C, there was no settling and the subsample was cut and placed flush with the top edge of the crucible.

2.6. Critical Shear Stress Measurement

[18] The critical shear stress was determined for replicate subsamples subjected to each temperature. These ranged from 40°C (maximum temperature assumed for samples in the field) to 550°C. The samples were composed of a mixture of particle sizes held together by both chemical and organic bonds. The criteria for the initiation of erosion of this soil matrix were therefore different than the criterion for initiation of erosion of noncohesive sediments used to calibrate the flume and depended upon the type of parent material and the temperature range. One of the following criteria for the initiation of erosion for cohesive, mixed-grain soils were observed after the initial winnowing of ash and fine sediment (less than about 0.125 mm) from the surface: (1) movement of the coarser sediment fraction (1–2 mm) over the finer fraction (typically 0.125–0.500 mm), as opposed to just winnowing of the fine fraction, and producing a coarse sediment lag on the surface; (2) steady erosion or scour of the surface, which has been referred to by *Luque and van Beek* [1976] as "nonceasing" scour; (3) erosion of several large (1–2 mm) soil aggregates in succession from the surface.

[19] The critical shear stress measurements were initiated at the lowest discharge (0.102 L s^{-1}) and with the flume level or with a slight positive (upward) slope. This positive slope helped to minimize the initial wave of water associated with starting the flow in the flume and decreased the

Table 3. Critical Shear Stress at Various Temperatures and Estimates of Cohesive Forces[a]

Temperature, °C	Hi Meadow (Granite) Mean ± 95% CL (*n*)	Pine Ridge (Sandstone) Mean ± 95% CL (*n*)	RMHRC (Granite) Mean ± 95% CL (*n*)	Rendija (Volcanic Tuffs) Mean ± 95% CL (*n*)	Sand (0.71–0.85 mm) Mean ± 95% CL (*n*)
			Critical Shear Stress, N m^{-2}		
40	2.2 ± 0.1 (22)	2.0 ± 0.2 (9)	1.2 ± 0.4 (11)	1.4 ± 0.2 (7)	0.45 ± 0.04 (4)
150	2.2 ± 0.2 (4)	1.9 ± 0.5 (7)	. . .	. . .	0.49 ± 0.04 (4)
175	. . .	. . .	0.9 ± 0.2 (4)	. . .	. . .
200	>3.2[b] (3)	1.9 ± 0.4 (5)	1.8 ± 0.4 (4)	. . .	0.50 ± 0.07 (4)
225	>3.2[b] (4)	. . .	>3.2[b] (4)	. . .	. . .
250	1.0 ± 0.3 (10)	. . .	1.1 ± 0.5 (4)	. . .	. . .
275	0.8 ± 0.7 (2)	0.8 ± 0.3 (3)	. . .	. . .	. . .
300	0.8 ± 0.1 (2)	. . .	. . .	. . .	. . .
325	. . .	. . .	0.6 ± 0.04 (4)	. . .	. . .
350	0.8 ± 0.1 (12)	. . .	. . .	. . .	. . .
400	. . .	0.7 ± 0.2 (4)	. . .	. . .	0.61 ± 0.07 (4)
450	0.5 ± 0.1 (3)	. . .	. . .	. . .	. . .
550	0.5 ± 0.1 (4)	0.6 ± 0.1 (4)	0.5 ± 0.03 (4)	0.5 ± 0.1 (7)	0.48 ± 0.05 (4)
			Estimate of Cohesive Force, N m^{-2}		
40	90	60	30	50	−10

[a]Abbreviations are as follows: *n*, number of replicates; CL, confidence limits.
[b]Some samples never eroded or eroded as large "chunks" greater than 50% of the sample.

net water surface slope and its associated shear stress below the critical value. The subsamples in the crucible were prewetted before the wooden insert with the crucible was placed on the floor of the flume. The porcelain crucible with the test sample was covered with a thin aluminum plate that was slowly withdrawn downstream after the flow in the flume had equilibrated. The slope of the flume was slowly increased (negatively, downward) until the ash (if any) and fine sediment began to move. The slope of the flume was calculated by measuring the vertical change relative to the level position of a light beam from a laser mounted on the top of the flume (Figure 1) and projected onto a wall located 7.82 m from the pivot point of the flume. The slope was then increased in increments until one of the three criteria listed above was observed. If none of the criteria was observed, the flow was stopped, the sample covered with the aluminum plate, and the procedure repeated at the higher discharge (0.505 L s^{-1}). If no initiation of erosion occurred at the higher discharge, then the maximum slope (−0.0461) was recorded. The maximum shear stress, corresponding to this maximum slope, calculated using the depth-slope product was 3.2 N m^{-2}.

[20] During the experimental runs we considered the time duration of the sediment response and chose to change the flume slope on a timescale of 5–10 s. We estimated the timescale for the turbulent fluctuations by applying Taylor's "frozen turbulence" hypothesis [*Tennekes and Lumley*, 1990] to shallow, turbulent flow. Flow depths were similar to hillslopes and ranged from 0.0020–0.018 m. Mean flow velocities (0.14–1.4 m s^{-1}) across the entire width of the flume were calculating using the water discharge (either 0.102 or 0.505 L s^{-1}), the flume width (0.083 m), and the flow depths and were on average about 20% less than those predicted assuming hydraulically smooth flow [*Middleton and Southard*, 1984] at the center of the flume. These velocities were used to compute the Reynolds number (1100–6500) and Taylor's timescale (0.003–0.070 s) or frequency (14–330 cycles s^{-1}). Turbulent fluctuations in this frequency range are too small in spatial scale and persist for too short a time to move soil particles out of their pocket, because of the inertia of the particles, and thus the timescale for changing the flume slope was many times greater than the turbulent timescales for the flume experiments and for those characteristic of flow on hillslopes.

[21] Sediment eroded during the measurement was caught in a 0.063 mm sieve (Figure 1), dried, and sieved to determine the distribution of particle sizes greater than 0.063 mm. Particles less than 0.063 mm passed through the sieve, became suspended sediment, and were removed when the flume was drained after each series of four replicate measurements. The suspended sediment never reached concentrations sufficient to affect the viscosity of the fluid. A total of 320 runs were made using different soils and at different temperatures to measure the critical shear stress, and 71 of these runs yielded data that could be used to determine the critical shear stress for the initiation of motion of ash. An additional 20 runs were made, as a control, to determine the effect of temperature on the critical shear stress for noncohesive sand (0.71–0.85 mm) similar to that used to calibrate the flume.

3. Results

[22] In general, the relation between critical shear stress and temperature can be separated into three different temperature ranges (<175°C; 175°C–275°C; >275°C) for the soil types that were tested. The critical shear stress was most variable (1.0–2.0 N m^{-2}) for temperatures less than 175°C, was a maximum (>2.0 N m^{-2}) between 175° and 275°C, and was essentially constant (0.5–0.8 N m^{-2}) for temperatures greater than 275°C (Figure 3). Critical shear stresses at 200° and 225°C for the Hi Meadow samples and at 225°C for the RMHRC sample exceeded the range of the calibration curve and were estimated to be greater than 3.2 N m^{-2} using the depth-slope product. These samples were cohesive and indurated after heating, failed to wet, and would either erode as one or two large chunks representing at least 30% of the sample or would fail to erode at the

maximum slope of the flume. The maximum slope occurred most frequently in testing samples in the 175°–275°C range and for the granitic soils (18% of Hi Meadow, 25% of RMHRC, and 8% of Pine Ridge samples). Samples of soil collected from natural burned sites were tested in the flume and had similar critical shear stresses. The Hayman sample had a critical shear stress of 1.7 ± 0.3 N m^{-2} (mean ± 95% confidence limits) and the Missionary sample had a critical shear stress of 1.8 ± 0.3 N m^{-2}. The critical shear stress for the control (sand sample, 0.71–0.85 mm) ranged from 0.45 to 0.61 N m^{-2} and had a maximum critical shear stress at a higher temperature (400°C) than the forest soils (Table 3 and Figure 3). The critical shear stress for ash was less than that for very fine noncohesive sand (0.19 N m^{-2}), and averaged 0.05 N m^{-2}.

[23] The median size of the eroded material did not depend on temperature but seemed to depend on soil type. The Hi Meadow sample suggested a slight decrease in size with increase in temperature (R^2 = 0.37), but both the Pine Ridge and RMHRC samples showed no change in size with temperature. In general, for the samples heated in the muffle furnace, the average ratio of the median size of the eroded sediment (>0.063 mm) to the median size of the same fraction (>0.063 mm) of the original sediment was about 1.0 (see Table 2). For the samples from natural burn sites, the average ratio was quite variable (0.3 ± 0.1 for the Hayman sample and 3.8 ± 0.3 for the Missionary sample).

4. Discussion

4.1. Laboratory and Field Conditions

[24] These laboratory results probably do not reproduce field conditions perfectly for several reasons. The ''gradual'' heating in the furnace over 1 hour may represent either too short or too long a duration when compared to heating duration times for wildfires. The heating process, while isotropic, is also different because heat in the muffle furnace penetrates the soil on all sides, while heat from wildfires can only penetrate from the surface downward producing a thermal gradient near the surface. The 1 hour exposure time in the muffle furnace coupled with the small sample size probable created drier antecedent soil conditions (less than 1%) than under natural conditions. The subsequent wetting of the subsamples just before the samples were put in the flume may have created greater soil moisture conditions than might be present during the first rainstorm after a fire. Another reason is that the sample size was necessarily small to permit heating in the muffle furnace and this small size created some edge effects around the crucible. However, to minimize these possible edge effects, observations of the erosion processes were focused across the central 0.010 m of the sample. Nevertheless, the errors associated with all of these potential problems are small relative to inherent structural variability in the soil and the fire characteristics.

4.2. Critical Shear Stress for Cohesive Material

[25] The question of the existence of a threshold or critical shear stress for cohesive materials has been debated in the literature with specific reference to marine sediments [*Lavelle and Mofjeld*, 1987]. Many unconsolidated marine sediments tend to act in a pseudo-plastic [*Johnson*, 1970] rather than a visco-plastic [*Prager*, 1961; *Furbish*, 1997] manner, making determination of a nonzero critical shear stress challenging. In contrast, the forest soils that we investigated appeared to yield viscoplastically or plastically rather than pseudo-plastically, and appeared to have a well defined, although not necessarily accurately resolved, critical shear stress. Keeping in mind the problem of the various criteria for critical shear stress, it is interesting to compare values from this paper with others published in the literature. For example, our critical shear stress measurements are similar to those (0.69 to 6.64 N m^{-2}) calculated by *Elliot et al.* [1989] and to those (0.50 to 1.27 N m^{-2}) calculated by *Zhu et al.* [2001] for agricultural soils using regression techniques. This suggests that for a wide variety of bare surfaces subjected to normal temperatures, the critical shear stresses are roughly the same.

4.3. Effect of Slope on Critical Shear Stress

[26] Owing to the role that particle weight plays in resisting particle motion, the critical shear stress for erosion depends on the slope of the surface. Consequently, a modification of the force balance for the initiation of particle motion is necessary to generalize the results of our experiments for use with cohesive soils on hillslopes, which are steeper than most stream channels. In the absence of this modification, the results presented in this paper can be considered maximum values. The additional resisting force is the cohesive force, $F_c = f_c A_s$ (where A_s is the surface area of the particle), and therefore this force is added to the right-hand side of equation (2). We set $\alpha_2 = 2A_s/A_x$ and note that α_2 is 8 for spherical and 6 for cubic particles. Thus equation (9) generalizes to

$$(\tau_b)_c = \frac{(\rho_s - \rho) g \alpha_1 D \cos\theta(\tan\phi_0 - \tan\theta) + \alpha_2 f_c}{I_R C_D \left[1 + \tan\phi_0 \left(\frac{C_L}{C_D} \frac{\left(f_T^2 - f_B^2\right)}{I_R}\right)\right]}. \quad (12)$$

[27] Our experiments show that unburned cohesive forest soils have critical shear stresses more than five time greater than those for noncohesive sediment even when tan θ is small. As tan θ increases, the difference between tan θ and tan ϕ_0 in (12) decreases causing the gravitational effects to decrease in magnitude even further relative to the cohesive effects. Consequently, on moderate to steep hillslopes, the gravitational effects can be neglected and no correction of our experimental results for slope is required. For low to moderate slopes, one needs to estimate the cohesive force, f_c. We used a particle size equivalent to the D_{50} of the soil type (which included the <0.063 mm size class and we used 0.5 mm for Rendija), substituted these parameters and constants (ϕ_1 = 67°; β = 0.3; C_L = 0.2; C_D = 0.85; α_1 = 4/3; θ = 0°; g = 9.8 ms^{-2}; ρ_s = 2650 kg m^{-3}; and ρ = 1000 kg m^{-3}) and the corresponding critical shear stresses (Table 3 for 40°C) into equation (12), and solved for the cohesive force per unit area (Table 3). The estimated cohesive force for the noncohesive sand sample (0.71–0.85 mm) is less than zero (Table 3) suggesting that the parameters of the noncohesive sediment, which were chosen were slightly in error. These same parameters were used to calculate the cohesive forces for the cohesive sediment and thus potentially introduced a negative bias of approximately 10 N m^{-2}. However, the order of magnitude of the cohesive

force per unit area for unburned soil is similar among soil types and one to two orders of magnitude greater than the critical shear stress at all temperatures. Using these values of f_c in equation (12) permits calculations of $(\tau_b)_c$ to be made using (12) for conditions other than the experimental ones, including low to moderate slopes. However, owing to the natural variability in f_c on forested hillslopes and its dominant effect on the critical shear stress for significant motion of soil particles, high accuracy in the evaluation of $(\tau_b)_c$ from (12) should not be expected.

[28] The primary focus of this paper is on burned soils, but when near-surface soil temperatures during the fire remain below about 175°C, the soils do not significantly change their cohesive properties. In this situation, the method described in the previous paragraph can be applied, and to a first approximation no slope correction need be made. Similarly, if the burned soils are granitic and they reach temperatures between 175° and 225°C (see Figure 3), the cohesion in these soils is such that $F_g' \ll F_c$ and equation (12) reduces to

$$(\tau_b)_c = \frac{\alpha_2 f_c}{I_R C_D \left[1 + \tan\phi_0 \left(\frac{C_L}{C_D}\frac{\left(f_T^2 - f_B^2\right)}{I_R}\right)\right]}. \quad (13)$$

In this case, all effects associated with particle weight, including those arising from the slope of the hillside, can be neglected. As a consequence, the flume results can be applied directly to any hillside in this intermediate thermal regime.

[29] In contrast, in the case of severely burned hillslopes (T > 275°C) composed of any type of sediment, $F_g' \gg F_c$, and the method of *Wiberg and Smith* [1987] can be used together with (1) the measured size distribution for the soil on the burned hillside and (2) the measured slope to obtain the critical shear stress of the burned soil. This calculation can be made for a hillslope of any steepness. In such calculations, a value for tan ϕ_0 is required, and, for significant sediment motion, it can be determined using $\phi_1 = 67°$ and $\beta = 0.3$, as described previously in the paper. The critical boundary shear stress for significant motion of soil particles measured in our flume, thus, can be applied directly to hillsides of any slope in situations where $F_g' \ll F_c$ and can be modified for application to hillsides of any slope when F_g' = order(F_c) or $F_g' \gg F_c$ using equation (12).

4.4. Erosion Processes

[30] Several types of erosion processes were observed for the naturally cohesive forest soils that had been subjected to different temperatures. At low temperatures (less than about 175°C) the soil surface had more variability in texture and distribution of organic material than at higher temperatures. These surface irregularities occasionally caused localized eddies and consequently localized erosion. The cohesive mechanisms span about three orders of magnitude from microscopic to macroscopic length scales [*Gerits et al.*, 1990]. Some of those on the macroscopic scale could be observed in the flume and are described here. For the unheated soils, organic filaments like rhizomes and rootlets often held soil aggregates together until the shear stress actually broke the filaments. Some samples like the sandstone samples (Pine Ridge and Missionary) had greater proportions of fines but were cohesive, and therefore, the first criterion (movement of coarse sediment on fine sediment) was not applicable and either criterion 2 or 3 was used to determine the initiation of erosion.

[31] In the temperature range between 175° and 275°C, many test samples appeared cemented or indurated and were difficult to prewet before testing in the flume. Frequently, these samples did not erode at all or large fractions eroded after fractures developed at the surface. For temperatures in the 175°–275°C range, some samples also were indurated and none of the erosion criteria were met; therefore, only a minimum critical shear stress (3.2 N m^{-2}) could be estimated. The actual critical shear stress for erosion could be an order of magnitude higher. Because the samples would not wet, air trapped under the surface would rise, and occasional air bubbles would escape from the sample, burst, and carry sediment into the flow. This ebullition process may be an important process of erosion after wildfire, especially during the first rainfall and runoff when natural soil also would respond similarly because of the drying and increased water repellency. The samples tested from two natural fire sites in Colorado (Hayman Fire and Missionary Ridge Fire, both in 2002) had similar critical shear stresses (1.7 and 1.8 N m^{-2}, respectively). On the basis of where these stresses would intersect the curves in Figure 3, the temperatures were probably between 225° and 250°C. This temperature range is an approximate, spatially averaged estimate of temperature during those wildfires. Localized spots where logs had burned on the ground producing white ash may have had higher temperatures and the orange-reddish color of the soil indicates temperatures greater than 350°C [*Ulery and Graham*, 1993]. These occasional areas of higher temperature typically are small in extent and thus would have little effect on the spatial average soil temperature.

[32] For samples subjected to temperatures greater than about 275°C in this study, the ash particles were the first to erode at a critical shear stress ~0.05 N m^{-2}, however, this was not considered to indicate erosion of the soil. Often the samples tested between about 275° and 350°C were coated with black soot, which was an indicator of the temperature and the incomplete combustion of the organic matter at those temperatures. At higher temperatures (>350°C), the samples were consistently an orange-reddish color indicating complete combustion and some iron oxidation of soil particles [*Ulery and Graham*, 1993]. At these high temperatures the organic material was absent, the surfaces were more uniform, and the soils were observed to be noncohesive. The bulk density of samples at these temperatures was about 20% less than that of the unheated samples. This decrease in bulk density is similar to the measured change in porosity of burned Mediterranean soils reported by *Imeson et al.* [1992]. As a result, these samples had a "puffy" texture, were noncohesive, and were eroded easily.

4.5. Similarity of Critical Shear Stress and Water Repellency Dependence on Temperature

[33] The changes in the critical shear stress with temperature parallel changes in water repellency observed in laboratory investigations [*DeBano and Krammes*, 1966; *DeBano*, 2000]. The critical shear stress was approximately constant in the low-temperature range (<175°C), and in

general, water repellency has been reported to be nearly constant [*DeBano*, 2000] with some degree of variability [*Dekker et al.*, 1998] in the same temperature range. Similarly, the critical shear stress was variable for different unburned soil types, which may reflect the hierarchy of different cohesive mechanisms with different magnitudes (Table 3).

[34] In the intermediate temperature range 175°–275°C, indurated soil samples were observed, values of the critical shear stress increased, and measurements of water repellency have been observed by *DeBano and Krammes* [1966] to reach a maximum. It is worthwhile, at this point, to examine the possible underlying causes for the increased water repellency and critical shear stress. The indurated samples were probably the result of a change in the type of cohesion or cementation. At temperatures less than 220°C, the cohesion is attributed to the organic cementation (organometallic compounds [*Giovannini et al.*, 1988] and polysaccharides produced by microorganisms and secreted by rootlets [*Gerits et al.*, 1990]). This organic cementation is destroyed at temperatures above 220°C [*Humphreys and Craig*, 1981; *Giovannini et al.*, 1988] and replaced by sesquioxide clay cementation, which involves iron, aluminum and titanium oxide clays [*Donahue et al.*, 1977] and has been compared to soil laterization [*Giovannini et al.*, 1988]. Sesquioxide clay cementation has been used to explain the increase in soil aggregate stability [*Giovannini and Lucchesi*, 1983; *Guerrero et al.*, 2001; *Mataix-Solera and Doerr*, 2004] and to explain the increase in sand and silt-size aggregates for soil samples tested in the laboratory after being subjected to temperatures from 25° to 900°C [*Wells*, 1981; *Giovannini et al.*, 1988; *Ulery and Graham*, 1993]. This cementation may explain the observed 3.8-fold increase ($p = 0.022$) in the median size of eroded material (compared to the original material >0.063 mm) after heating for the Missionary sample and the slight 1.1-fold increase ($p = 0.069$) in particle size for the Pine Ridge sample. Both samples, but especially the Missionary sample, had fine material (Table 2) that could be cemented to produce larger aggregates. Surprisingly, the uniform, noncohesive sand (0.71 to 0.85 mm) also showed a significant maximum in critical shear stress at 400°C (Figure 3). This may have been a result of a residue of clay particles adsorbed to the sand grains even after the sand was washed and sieved. The sand particles on the surface of the test samples were definitely aggregated and water repellent, when the sand was first exposed to flowing water after removal of the protective aluminum plate. The physiochemical changes in cohesion are speculative but the measured increased in magnitude of the cohesion and water repellency has important consequences. In general, in this temperature range (220°–275°C), all landscapes (especially those with granitic soils) will be less erodible, and thus, primarily a source of water, ash, and fine sediment rather than coarse sediment. The excess water flowing off hillslopes into drainages and channels will erode most of the coarse sediment. This is supported by field measurements made after the Buffalo Creek Fire in Colorado [*Moody and Martin*, 2001a, 2001b] where 20% of the eroded sediment was estimated to have originated from hillslopes and 80% from drainages and channels.

[35] The critical shear stress for all soils decreased abruptly to about 0.8 N m^{-2} in the upper temperature range (>275°C) and then decreased slowly to about 0.5 N m^{-2} near 550°C. Similarly, water repellency also has been observed to decrease and soil porosity to increase when temperatures were greater than about 280°C [*DeBano*, 2000]. Again, the possible underlying causes for the similar response of critical shear stress and water repellency may be explained by the physiochemical changes in cohesion. The increase in porosity has been attributed to the combustion of organic matter [*Humphreys and Craig*, 1981] and the fusion of finer clay particles into aggregates [*Giovannini et al.*, 1988]. This increase in porosity has been observed in the field [*Imeson et al.*, 1992] and in the laboratory by the authors based on the texture of the samples after heating and before testing. At temperatures greater than 460°C, some clay minerals lose hydroxyl groups [*Giovannini et al.*, 1988] causing the crystallographic structure to collapse resulting in a decrease in sesquioxide clay cementation, which further increases the soil porosity and erodibility. Thus the destruction of sesquioxide clay cementation may explain why the critical shear stress has a narrow range (0.5–0.8 Nm^{-2}) and is essentially constant over this upper temperature range (>275°C).

[36] This relation between critical shear stress and temperature has important consequences for modeling erosion on a watershed scale after wildfire. For unburned soils the spatial variability of soil erodibility has been mapped at the watershed scale (0.01–10 km^2) and at the landscape scale (10–10^6 km^2) using the Universal Soil Loss Equation's K-factor [*Renard et al.*, 1997]. These maps show a complex spatial distribution and a relatively wide range in magnitudes (K-factor = 0.1–2.0 m^{-1}) for soil types in the region west of the Great Plains of the United States [*Wolock*, 1997]. The results in this paper indicate that wildfire reduces this complex spatial variability to a much simpler spatial pattern that is independent of soil type and primarily reflects the spatial distribution of maximum soil temperature. When maximum soil temperatures are 175°–275°C, the critical shear stress is relatively high (>2 N m^{-2}), the soils are indurated, and the soil erodibility can be modeled as minimal. When maximum temperatures are greater than 275°C, the range in magnitude of the critical shear stress (0.5–0.8 N m^{-2}) is narrow and the erodibility can be modeled as the same for all soil types.

5. Conclusions

[37] Critical shear stress for the initiation of erosion of forest soils has a complex dependence on temperatures within the range typically measured in wildfires. In general, the relation between critical shear stress and temperature can be separated into three different temperature ranges (<175°C; 175°C–275°C; >275°C) for the soil types that were tested. The critical shear stress was most variable (1.0–2.0 N m^{-2}) for temperatures less than 175°C, was a maximum (>2.0 N m^{-2}) between 175° and 275°C, and was essentially constant (0.5–0.8 N m^{-2}) for temperatures greater than 275°C. The similarities in the changes in critical shear stress with temperature and the changes in water repellency with temperature suggest that the two soil properties are linked. This link may be through the types of cementation processes exhibited by cohesive mixed-grain soils at different temperatures.

[38] In general, the changes in critical shear stress with temperature shown in this paper are independent of soil type and suggest that erosion processes in burned watersheds can be modeled more simply than erosion processes in unburned watersheds. Wildfire reduces the complex spatial variability of soil erodibility associated with unburned watersheds by eliminating the complex vegetation component of erosion and by reducing the range of critical shear stresses associated with different types of unburned soils. In addition, when these results are applied to watersheds with steep, burned hillslopes, the range of critical shear stress will be reduced even more by the effect of the down slope component of gravity. Thus predicting the erosional response after a wildfire will depend primarily on determining the distribution of the maximum soil temperatures that were reached during the wildfire. At the present time maximum soil temperatures are not mapped. However, even initial low-resolution (~40 ha) soil burn severity maps based on infrared photographs (A. Parsons, written communication, 2003) provide some indirect estimate of the spatial distribution of maximum soil temperature and more recent high-resolution (0.0006–0.09 ha) soil burn severity maps based on remote sensing of visible and near infrared radiation provide more spatially detailed estimates of maximum soil temperature.

References

Ashida, K., and M. Bayazit (1973), Initiation of motion and roughness of flows in steep channels, paper presented at the 15th Congress, Int. Assoc. for Hydraul. Res., Istanbul.

Bathurst, J. C., W. H. Graf, and H. H. Cao (1987), Bed load discharge equations for steep mountain rivers, in *Sediment Transport in Gravel-Bed Rivers*, edited by C. R. Thornes et al., chap. 15, pp. 453–491, John Wiley, Hoboken, N. J.

Croad, R. N. (1981), Physics of erosion of cohesive soils, Ph.D. thesis, Dep. of Civil Eng., Univ. of Auckland, New Zealand.

DeBano, L. F. (1969), Observations on water-repellent soils in western United States, in *Water-Repellent Soils, Proceedings of the Symposium on Water-Repellent Soils*, edited by L. F. Debano and J. Letey, pp. 17–29, Univ. of Calif., Riverside.

DeBano, L. F. (2000), The role of fire and soil heating on water repellency in wildland environment: A review, *J. Hydrol.*, *231–232*, 195–206.

DeBano, L. F., and C. E. Conrad (1978), The effect of fire on nutrients in a chaparral ecosystem, *Ecology*, *59*, 489–497.

DeBano, L. F., and J. S. Krammes (1966), Water repellent soils and their relation to wildfire temperature, *Bull. Int. Assoc. Sci. Hydrol.*, *11*, 14–19.

Dekker, L. W., C. J. Ritsema, K. Oostindie, and O. H. Boersma (1998), Effect of drying temperature on the severity of soil water repellency, *Soil Sci. Soc. Am. J.*, *163*, 780–796.

Dekker, L. W., S. H. Doerr, K. Oostindie, A. K. Ziogas, and C. J. Ritsema (2001), Water repellency and critical soil water content in a dune sand, *Soil Sci. Soc. Am. J.*, *65*, 1667–1674.

Doehring, D. O. (1968), The effect of fire on geomorphic processes in the San Gabriel Mountains, California, in *Contributions to Geology*, edited by R. B. Parker, pp. 43–65, Univ. of Wyo. Press, Laramie.

Doerr, S. H., R. A. Shakesby, and R. P. D. Walsh (2000), Soil water repellency: Its causes, characteristics and hydro-geomorphological significance, *Earth Sci. Rev.*, *5*, 33–65.

Donahue, R. L., R. W. Miller, and J. C. Shickluna (1977), *Soils: An Introduction to Soils and Plant Growth*, 626 pp., Prentice-Hall, Upper Saddle River, N. J.

Elliot, W. J., A. M. Liebenow, J. M. Laflen, and K. D. Kohl (1989), A compendium of soil erodibility data from WEPP cropland soil field erodibility experiments 1987 & 88, *NSERL Rep. 3*, Ohio State Univ. and U.S. Dep. of Agric. Agric. Res. Serv., U.S. Govt. Print. Off., Washington, D. C.

Flanagan, D. C., and M. A. Nearing (1995), USDA-Water Erosion Prediction Project: Hillslope profile and watershed model documentation, *NSERL Rep. 10*, U.S. Dep. of Agric. Agric. Res. Serv., Natl. Soil Erosion Res. Lab., West Lafayette, Ind.

Furbish, D. J. (1997), *Fluid Physics in Geology: An Introduction to Fluid Motions on Earth's Surface and Within Its Crust*, 476 pp., Oxford Univ. Press, New York.

Gerits, J. J. P., J. L. M. P. de Lima, and T. M. W. van den Broek (1990), Overland flow and erosion, in *Process Studies in Hillslope Hydrology*, edited by M. G. Anderson and T. P. Burt, chap. 6, pp. 173–191, John Wiley, Hoboken, N. J.

Giovannini, G., and S. Lucchesi (1983), Effect of fire on hydrophobic and cementing substances of soil aggregates, *Soil Sci.*, *136*, 231–236.

Giovannini, G., S. Lucchesi, and M. Giachetti (1988), Effect of heating on some physical and chemical parameters related to soil aggregation and erodibility, *Soil Sci.*, *146*, 255–261.

Govers, G. (1987), Initiation of motion in overland flow, *Sedimentology*, *34*, 1157–1164.

Guerrero, C., J. Mataix-Solera, J. Navarro-Pedreño, F. García-Orenes, and I. Gómez (2001), Different patterns of aggregate stability in burned and restored soils, *Arid Land Res. Manage.*, *15*, 163–171.

Hairsine, P. B. (1988), A physically-based model of the erosion of cohesive soils, Ph.D. thesis, 287 pp., Griffith Univ., Brisbane, Queensland, Australia.

Hanson, G. J. (1991), Development of a jet index to characterize erosion resistance of soil in earthen spillways, *Trans. Am. Soc. Agric. Eng.*, *34*, 2015–2020.

Hartley, D. M., and P. Y. Julien (1992), Boundary shear stress induced by raindrop impact, *J. Hydraul. Res.*, *30*, 341–359.

Helvey, J. D. (1980), Effects of a north central Washington wildfire on runoff and sediment production, *Water Resour. Bull.*, *16*, 627–634.

Humphreys, F. R., and F. G. Craig (1981), Effects of fire on soil chemical, structural and hydrological properties, in *Fire and the Australian Biota*, edited by A. M. Gill et al., chap. 8, pp. 177–200, Aust. Acad. Sci., Canberra.

Imeson, A. C., J. M. Verstraten, E. J. van Mulligen, and J. Sevink (1992), The effects of fire and water repellency on infiltration and runoff under Mediterranean type forest, *Catena*, *19*, 345–361.

Johnson, A. M. (1970), *Physical Processes in Geology*, 577 pp., W. H. Freeman, New York.

Johnson, E. A., and K. Miyanishi (Eds.) (2001), *Forest Fires Behavior and Ecological Effects*, 600 pp., Elsevier, New York.

Koorevaar, P., G. Menelik, and C. Dirksen (1983), *Elements of Soil Physics*, 228 pp., Elsevier, New York.

Lavelle, J. W., and H. O. Mofjeld (1987), Do critical stress for incipient motion and erosion really exist?, *J. Hydraul. Eng.*, *113*, 370–390.

Luque, R. F., and R. van Beek (1976), Erosion and transport of bed-load sediment, *J. Hydraul. Res.*, *14*, 127–144.

Massman, W. J., J. M. Frank, W. D. Shepperd, and M. J. Platten (2003), In situ soil temperature and heat flux measurements during controlled surface burns at a southern Colorado forest site, *For. Serv. Proc. RMRS-P-29*, U.S. Dep. of Agric., Washington, D. C.

Mataix-Solera, J., and S. H. Doerr (2004), Hydrophobicity and aggregate stability in calcareous topsoils from fire-affected pine forest in southeastern Spain, *Geoderma*, *118*, 77–88.

Meyer-Peter, E., and R. Müller (1948), Formulas for bed-load transport, paper presented at the 2nd Meeting, Int. Assoc. for Hydraul. Res., Stockholm.

Middleton, G. V., and J. B. Southard (1984), *Mechanics of Sediment Movement*, 401 pp., Soc. of Econ. Paleontol. and Mineral., Tulsa, Okla.

Miller, R. L., and R. J. Byrne (1966), The angle of repose for a single grain on a fixed rough bed, *Sedimentology*, *6*, 303–314.

Miller, M. C., I. N. McCave, and P. D. Komar (1977), Threshold of sediment motion under unidirectional currents, *Sedimentology*, *24*, 507–527.

Moody, J. A., and D. A. Martin (2001a), Initial hydrologic and geomorphic response following a wildfire in the Colorado Front Range, *Earth Surf. Processes Landforms*, *26*, 1049–1070.

Moody, J. A., and D. A. Martin (2001b), Hydrologic and sedimentologic response of two burned watersheds in Colorado, *U.S. Geol. Surv. Water Resour. Invest. Rep., 10-4122*, 142 pp.

Morgan, R. P. C. (1986), *Soil Erosion and Conservation*, 296 pp., John Wiley, Hoboken, N. J.

Moss, A. J., and P. Green (1983), Movement of solids in air and water by raindrop impact, effects of drop-size and water-depth variation, *Aust. J. Soil Res.*, *21*, 257–269.

Nearing, M. A. (1991), A probabilistic model of soil detachment by shallow turbulent flow, *Trans. Am. Soc. Agric. Eng.*, *34*, 81–85.

Nearing, M. A., L. D. Norton, D. A. Bulgakov, G. A. Larionov, L. T. West, and K. M. Dontsova (1997), Hydraulics and erosion in eroding rills, *Water Resour. Res.*, *33*, 865–876.

Neary, D. G., C. C. Klopatek, L. F. DeBano, and P. F. Ffolliott (1999), Fire effects on belowground sustainability: A review and synthesis, *For. Ecol. Manage.*, *122*, 51–71.

Poesen, J., and J. Savat (1981), Detachment and transportation of loose sediments by raindrop splash, part II, Detachability and transportability measurements, *Catena*, *8*, 19–41.

Prager, W. (1961), *Introduction to Mechanics of Continua*, 230 pp., Ginn, Chicago, Ill.

Raudkivi, A. J., and S. K. Tan (1984), Erosion of cohesive soils, *J. Hydraul. Res.*, *22*, 217–233.

Reichardt, H. (1951), Vollstandige Darstellung der turbulenten Geschwindigkeitsverteilung in glatten Leitungen, *Z. Angew. Math. Mech.*, *31*, 208–219.

Renard, K. G., G. R. Foster, G. A. Weesies, D. K. McCool, and D. C. Yoder (1997), Predicting soil erosion by water: A guide to conservation planning with the revised universal soil loss equation (RUSLE), *Agric. Handbook 703*, 404 pp., U.S. Dep. of Agric., Washington, D. C.

Robichaud, P. R., and R. D. Hungerford (2000), Water repellency by laboratory burning of four northern Rocky Mountain forest soils, *J. Hydrol.*, *231–232*, 207–219.

Rose, C. W., J. R. Williams, G. C. Sander, and D. A. Barry (1983), A mathematical model of soil erosion and deposition processes: I. Theory for a plane land element, *Soil Sci. Soc. Am. J.*, *47*, 991–995.

Shields, A. (1936), Anwendung der Ahnlichkeitsmechanik und der Turbulenzforschung auf die Geschiebebewegung, Mitteilungen der Preuss. Versuchsnst. F. Wasserbau u. Schiffbau, Heft 26, Berlin.

Shimizu, Y. (1989), Effects of lateral shear stress in open-channel flow, report, 22 pp., River Hydraul. and Hydrol. Lab., Civ. Eng. Res. Inst., Hokkaido, Japan.

Tennekes, H., and J. L. Lumley (1990), *A First Course in Turbulence*, 300 pp., MIT Press, Cambridge, Mass.

Ulery, A. L., and R. C. Graham (1993), Forest fire effects on soil color and texture, *Soil Sci. Soc. Am. J.*, *57*, 135–140.

Wells, W. G., II (1981), Some effects of brushfires on erosion processes in coastal southern California, *IAHS Publ.*, *132*, 305–342.

Wiberg, P. L., and J. D. Smith (1987), Calculations of the critical shear stress for motion of uniform and heterogeneous sediments, *Water Resour. Res.*, *23*, 1471–1480.

Wolock, D. M. (1997), STATSGO soil characteristics for the conterminous United States, *U.S. Geol. Surv. Open File Rep., 97-656*, 17 pp.

Yalin, M. S., and E. Karahan (1979), Inception of sediment transport, *J. Hydraul. Div.*, *105*, 1433–1443.

Yang, C. T. (1973), Incipient motion and sediment transport, *J. Hydraul. Div.*, *99*, 1679–1704.

Zhu, J. C., C. J. Gantzer, S. H. Anderson, R. L. Peyton, and E. E. Alberts (2001), Comparison of concentrated-flow detachment equations for low shear stress, *Soil Tillage Res.*, *61*, 203–212.

J. A. Moody and J. D. Smith, U. S. Geological Survey, 3215 Marine Street, Suite E-127, Boulder, CO 80303, USA. (jamoody@usgs.gov; jdsmith@usgs.gov)

B. W. Ragan, Department of Geosciences, Boise State University, Boise, ID 83725, USA. (brianragan@mail.boisestate.edu)